Published in final edited form as:
J Theor Biol. 2007 July 7; 247(1): 23–35.

Modeling the mechanisms of acute hepatitis B virus infection

Stanca M. Ciupe[*], **Ruy M. Ribeiro**[†], **Patrick W. Nelson**[‡], and **Alan S. Perelson**[*,†,0]

*****Santa Fe Institute, 1399 Hyde Park Rd., Santa Fe, NM, 87507*

†Theoretical Biology and Biophysics Group, Theoretical Division, Los Alamos National Laboratory, Los Alamos, NM 87545

‡Dept. of Mathematics, University of Michigan, 5860 E. Hall, Ann Arbor, MI 48109

Abstract

Mathematical models have been used to understand the factors that govern infectious disease progression in viral infections. Here we focus on hepatitis B virus (HBV) dynamics during the acute stages of the infection and analyze the immune mechanisms responsible for viral clearance. We start by presenting the basic model used to interpret HBV therapy studies conducted in chronically infected patients. We then introduce additional models to study acute infection where immune responses presumably play an important role in determining whether the infection will be cleared or become chronic. We add complexity incrementally and explain each step of the modeling process. Finally, we validate the model against experimental data to determine how well it represents the biological system and, consequently, how useful are its predictions. In particular, we find that a cell-mediated immune response plays an important role in controlling the virus after the peak in viral load.

1 Introduction

Hepatitis B virus infects liver cells (hepatocytes) and can cause both acute and chronic disease. It is believed that host factors, in particular immune responses, are responsible for determining whether the infection is cleared or becomes chronic (Thimme et al., 2003). In Figure 1 we show a typical profile of HBV viral load during acute infection.

Mathematical models have been used to help understand the dynamics of viral infections, such as human immunodeficiency virus and hepatitis C infection (see Perelson, 2002;Perelson et al., 2005 for reviews). Following these approaches, dynamic models were developed to analyze the changes in hepatitis B virus levels during drug therapy (Nowak et al., 1996;Tsiang et al., 1999;Lau et al., 2000;Lewin et al., 2001;Colombatto et al., 2006). These models typically considered uninfected (T) and infected (I) hepatocytes and free virus (V). They assumed that target cells, *i.e.*, cells susceptible to infection, are produced at a constant rate λ, die at per capita rate d, and become infected at a rate kTV, proportional to both the target cell concentration and the virus concentration. Infected hepatocytes are thus produced at rate kTV and are assumed to die at constant rate δ per cell. Upon infection, hepatocytes produce virus at rate p per infected cell, and virus is cleared at rate c per virion. The dynamics of the system are governed by the following equations

0Correspondence: Theoretical Division, Los Alamos National Laboratory, Los Alamos, NM 87545, Email: asp@lanl.gov, Phone: 505-667-6829, Fax: 505-665-3493

$$\frac{dT}{dt} = \lambda - dT - kVT,$$
$$\frac{dI}{dt} = kVT - \delta I, \quad (1)$$
$$\frac{dV}{dt} = pI - cV,$$

Several studies (Nowak et al., 1996;Tsiang et al., 1999;Lau et al., 2000;Lewin et al., 2001) have modified equation (1) to include antiviral therapy. The models introduced a therapy-induced block in virus production with efficacy ε, *i.e.*, replaced the term pI with $(1-\varepsilon)pI$, and a block in viral infection with efficacy η, *i.e.*, replaced the term kVT with $(1-\eta)kVT$. The models were then fit to viral load data from patients under therapy and patient specific parameters were estimated (see Ribeiro et al., 2002 for details).

None of these models (Nowak et al., 1996;Tsiang et al., 1999;Lau et al., 2000;Lewin et al., 2001) includes hepatocyte proliferation, although (Colombatto et al., 2006) includes homeostasis and thus keeps the number of infected plus uninfected hepatocytes constant. Although these various models allowed for a higher death rate of infected cells, presumably an effect of the immune response, none of them explicitly considered the immune dynamics and its cytolytic effects. Lewin et al. (2001) include the possibility of non-cytolytic infected cell cure, but it played no role in the viral dynamics under treatment. In another modeling approach, Payne et al. (1994a) looked at the conditions for different disease outcomes (self-limiting, chronic, recurring, hepatocellular carcinoma), based on the London-Blumberg model (Payne et al., 1994b), which postulates different types of hepatocytes. The driver for the different outcomes was the death rate of infected hepatocytes, which the authors interpreted as a surrogate marker for the strength of the immune system, without explicitly considering it. In addition, they presented this as a conceptual model for the long-term outcome of infection, without any specific patient data.

In this paper we modify equation (1) for the study of hepatitis B virus acute infection (Figure 1). In model (1) target cell limitation causes the decay in the virus concentration after the peak of infection, and this aspect was used successfully in the study of HIV primary infection (Perelson et al., 1996;Phillips, 1996;Stafford et al., 2000). However, preliminary work showed that model (1) was not sufficient to fit the viral load in acute HBV infection (Figure 2), where the virus is spontaneously cleared in 90% of adult patients (Chisari and Ferrari, 1995;Guidotti and Chisari, 2006). In this situation, the immune response is thought to play a crucial role in both viral clearance and disease pathogenesis. The immune response can lead to either “cure” of infected cells through down-regulation of HBV covalently closed circular DNA (cccDNA), the template for viral replication, and other replicative intermediates, which carry the genetic information of the virus (Guidotti et al., 1999;Wieland et al., 2004), or to the killing of infected hepatocytes mainly by HBV-specific $CD8^+$ T-lymphocytes (cellular immune response). The $CD8^+$ T-lymphocyte mediated killing of hepatocytes (Thimme et al., 2003) is compensated for by the liver's capacity to self renew, and hepatocyte proliferation replaces cells killed by the immune response (Summers et al., 2003). Explaining the mechanisms of viral clearance while maintaining liver integrity is fundamental in understanding HBV pathogenesis.

Below, we explicitly incorporate immune responses as well as hepatocyte proliferation into model (1), in various ways. We then use these new models to describe clinical data of acute infection in adult patients and to investigate the role of the immune response in disease outcome.

2 Model development

We consider five populations, corresponding to uninfected hepatocytes (T), two families of infected hepatocytes (I_1 and I_2), free virus (V), and immune system effector cells (E). Because liver size is maintained by homeostatic mechanisms, we assume that proliferation of uninfected target cells (T) is described by a logistic term with maximum proliferation rate r and carrying capacity T_{max}. When HBV infects a cell, the viral DNA is converted into a single covalently closed circular DNA (cccDNA) molecule. This is followed by accumulation of additional, up to 50 copies of cccDNA (Tuttleman et al., 1986). The amplification is caused by either synthesis pathways or by multiple infection events. We consider two classes of infected cells, those with one copy of cccDNA (I_1), and those with multiple copies of cccDNA (I_2). I_1 cells are produced at rate kTV, and are lost by division at rate r, by a non-cytolytic process that leads to "cure" of the infection at rate ρ_1 and recovery into the uninfected cell population, or by synthesis of new cccDNA and transition into the I_2 class at rate z. Later we will consider the possibility of multiple infections during transition from I_1 to I_2. Cells with multiple copies of cccDNA can lose these and eventually move into the population of cells with only one cccDNA copy; we assume that the average rate for this process is ρ_2. Transitions from I_2 to T have a small chance of occurrence, and we neglect them. Both types of infected cells proliferate in a manner similar to the uninfected cells. However, when an I_1 cell divides it will generate one infected cell with one copy of cccDNA and one cell with no cccDNA, since cccDNA is not replicated during cell division. Thus, the number of I_1 cells is not affected by cell division, but the number of uninfected cells increases. Both families of infected cells are killed by cytolytic cells at rate μE per cell. Free virus is produced at rates p_1 and p_2 by cells in class I_1 and I_2, respectively, and is cleared at rate c.

We assume, according to experimental evidence, that in the absence of infection there is a basal level of effector cells or effector cell precursors, given simply by s/d_E, where s corresponds to a source of $CD8^+$ T cells specific for HBV and d_E is the per capita loss rate of effector cells. Upon infection, the immune response is activated and effector cells expand at rate $\alpha(I_1 + I_2)E$, which depends on the number of infected cells. We also allow for a lag between infection and the $CD8^+$ T cell response in the liver as observed in HBV infection (Webster et al., 2000b) and other infections (Flynn et al., 1998;Nelson et al., 2000;Thimme et al., 2002;Davenport et al., 2004;Ciupe et al., 2006). To model this lag, we introduce a time delay in the activation and expansion of effectors E. That is, immune activation and clonal expansion at time t depends on the number of infected cells and effector cells at time $t - \tau$. The lag takes into consideration the time needed for antigen processing, antigen presentation, encounter between antigen presenting cells and antigen-specific CD8+ T cells, and ultimately their activation and movement from lymphoid tissue into the liver. For simplicity, we have not distinguished between effector cell precursors and fully differentiated effector cells. At their basal level these "effector" cells have little impact on the infection and it is only when these cells expand that their effect is observed.

The dynamics of acute infection are thus governed by the following equations:

$$\begin{aligned}
\frac{dT}{dt} &= r(T + I_1)(1 - \frac{T + I_1 + I_2}{T_{max}}) - kVT + \rho_1 I_1,\\
\frac{dI_1}{dt} &= kVT - (\rho_1 + z)I_1 - \mu I_1 E + \rho_2 I_2,\\
\frac{dI_2}{dt} &= rI_2(1 - \frac{T + I_1 + I_2}{T_{max}}) + zI_1 - \rho_2 I_2 - \mu I_2 E,\\
\frac{dV}{dt} &= p_1 I_1 + p_2 I_2 - cV,\\
\frac{dE}{dt} &= s + \alpha(I_1(t - \tau) + I_2(t - \tau))E(t - \tau) - d_E E.
\end{aligned} \tag{2}$$

2.1 Clinical data

HBV DNA measurements and serum alanine aminotransferase (ALT) (a marker of hepatocyte death) were obtained from the serum of seven patients acutely infected with the same HBV variant from a single source outbreak (Webster et al., 2000a,b).

Initially viral load increases exponentially, reaching a peak of up to 10^{10} HBV DNA copies per ml. The HBV level then declines in a biphasic manner, and seems to approach a plateau around 6 months post-infection (Figure 1). However, patients 1 through 6 cleared the infection at some later time, whereas patient 7 developed chronic HBV infection (Webster et al., 2000a,b).

2.2 Parameter estimation

We use literature values for some of the parameters of our model (Table 1). This reduces the degrees of freedom in fitting the model to data, and allows a better estimation of the remaining parameters.

To estimate the remaining parameters α, z, μ, τ, $\rho_{1,2}$, $p_{1,2}$ and k we used a hill climbing Monte Carlo algorithm (see Ciupe et al., 2006 for details). It searches over the space of all parameters to find the best fit of the model to the patients' data. The results are listed in Table 2.

3 Numerical results

Using the approach described above, we obtained good fits of model (2) to the data (Figure 3). The fitting procedure resulted in a biphasic decay pattern in the viral load in all patients. In Table 2, we present the parameter estimates corresponding to the best fits. There is little variation between the parameter values ρ_1 and ρ_2 among patients, which implies that the recovery rate from infected to uninfected cells is, on average, similar to the transition rate from I_2 to I_1. Virion production from infected cells in class I_2 is larger than from class I_1 with an average of 213 ± 157 virions/cell/day versus 102 ± 81 virions/cell/day, respectively.

The average fraction of infected cells at the peak of infection is 97% of total hepatocytes (Figure 4), with the majority of infected cells having multiple copies of cccDNA. The one exception is patient 6, who had a very small transition rate from I_1 to I_2 ($z = 0.22$ day^{-1}), resulting in 47% of the cells in class I_1. Our results show that an average 81±15% of hepatocytes have more than one cccDNA molecule. After the peak, the number of infected cells declines quickly, although with a somewhat slower decline in patient 7 (Figure 4).

The estimated mean delay in HBV-specific $CD8^+$ T-cell activation, τ, is 23 ± 5 days, with the longest delay of more than 4 weeks for patient 7. The rapid and sharp fall in HBV DNA levels took place an average of 43 ± 11 days before the peak in $CD8^+$ T-cell numbers (Figure 3).

The clinical study also recorded the concentration over time of alanine aminotransferase (ALT), a liver enzyme present in the blood of an individual that is a surrogate marker of hepatocyte damage (Gilles Feutren and Bach, 1984). Without designing a model for the ALT dynamics, we compared the measured ALT levels to the level of the cell-mediated immune response, E. There is a good correlation between the effector cell and ALT levels (Figure 3). This correspondence between the measured increase in ALT levels and our computed change in effector cell number suggests that our model is appropriately capturing the dynamics of the cell-mediated immune response.

4 Alternative models

4.1 Models of superinfection

In the model given by equation (2), we assumed that the increase in the pool of cccDNA inside an infected hepatocyte occurs in an infection independent manner, presumably due to newly synthesized relaxed circular DNA entering the nucleus. Since most cells are infected, as shown above, and there is continued production of virus, we also tested the possibility that cccDNA accumulation is due to superinfection of hepatocytes. In this model, all other assumptions are kept as before, except that the transition of infected cells from class I_1 into class I_2 no longer occurs at rate zI_1 as in model (2), but rather occurs by superinfection of I_1, *i.e.*, at rate zVI_1, proportional to the viral load. That is, multiple copies of cccDNA result from multiple infection events (Figure 5). There was a consistent improvement in the viral load fits during the second phase decay compared to the model given by equation (2) (see Table 3(a)), with a reduction of up to 37% in the residual sum of squares.

We note that the estimates for superinfection rate (z) are of the same order of magnitude as the initial infection rate, k. This seems to support the biological relevance of a superinfection scenario. A median of 94% cells were infected at the peak, out of which a median of 81% have multiple copies of cccDNA. These estimates are slightly lower than the ones predicted by the model given by equation (2).

4.2 Models of $CD8^+$ dependent non-cytolytic immune responses

We next examined the possibility that the non-cytolytic recovery of infected cells is $CD8^+$ T cell mediated, since $CD8^+$ T-cells produce cytokines that can induce the degradation of replicative intermediates and possibly the cccDNA from infected cells (Thimme et al., 2003). This is incorporated into the model given by equation (2), by letting the non-cytolytic recovery rates also depend on E, *i.e.*, $\rho_{1,2} = \rho_{1,2} + \rho'_{1,2}E$ (Figure 6). Using an F-test to compare the models with $\rho'_i = 0$ and $\rho' i \neq 0$, there is no statistically significant improvement in the fits, *i.e.*, p-values range between 0.26 and 1 among the patients with the exception of patient 6, for which p=0.02 (Table 3(b)). We calculated that the maximum value of $\rho'_{1,2}E$, attained when E reaches its maximum, was at least 2-logs lower than the corresponding value of $\rho_{1,2}$. And the effect of this E-dependent non-cytolytic effect was much lower at all other times. Thus, the inclusion of this effect does not noticeably influence the fits, nor does it influence the total number of cured hepatocytes.

4.3 Model with only one class of infected cells

One important biological characteristic in HBV infection is that each infected hepatocyte may have multiple copies of HBV cccDNA. We explicitly included this in a simplified manner in our model by considering two classes of infected cells. Many prior model have only consider one class of infected cells (Nowak et al., 1996;Tsiang et al., 1999;Lewin et al., 2001;Perelson and Ribeiro, 2004). Thus, we also fit a simpler model, with just one class of infected cells to the data. The results are presented in Figure 7 and Table 3(c). Inspection of the HBV viral load fits does not reveal any significant loss of quality in the fits in this model compared with the

model given by equation (2). This is in spite of the fits being up to 20% worse, measured by comparing the sum of squared residuals for individual patients between the two models. However, when we take into account that this model has only 6 parameters to fit, instead of 9, there is no statistical difference with the more complex model, by an F-test ($0.1 < P < 1$, Table 3(c)).

We also compared this model with the model in section 4.1 that includes superinfection, which presented a better overall fit to the data. Although these two models are not nested and thus can not be compared directly by an F-test, we compared them using the Akaike information criterion (AIC) (see Table 3a, for AIC of the model in section 4.1). For patients 4 and 5, the current model has considerable worse AIC scores; whereas for patients 3 and 7 the AIC scores are similar; finally for the remaining three patients the current model leads to better AIC. Thus, with this dataset, it is difficult to draw conclusions as to which model is better.

4.4 Cytotoxic immune response models

During acute viral infections, the $CD8^+$ T cell population dynamics is characterized by three distinct phases, a proliferation phase in which effector cells are generated, followed by a contraction phase when up to 95% of those cells undergo apoptosis, and a long memory phase (Lau et al., 1994;Asano and Ahmed, 1996;Zimmerman et al., 1996;Butz and Bevan, 1998).

In the model given by equation (2), we have simplified this process by considering the effector class, E, to represent the activated $CD8^+$ T cells responsible for the cytotoxic killing of infected hepatocytes, and we focused on the role of the delay in their expansion. At the start of the infection 0.01% or less of the total number of $CD8^+$ T cells are HBV-specific. This frequency was determined by Webster et al. (2000b) based on the percentage of HBV-specific $CD8^+$ T cells present in the responding population (see also Ogg and McMichael, 1998). However at the start of the infection these cells are probably naive, not activated.

To more accurately model the $CD8^+$ response, we consider the antigen-specific $CD8^+$ T cells to be either naive, N, or activated, E. Naive cells are produced at a constant rate s_N, die at rate d_N or become activated at rate ω. Activated cells proliferate at rate r_E and die at rate d_E. Since we are only modeling acute infection we do not consider that some activated cells can differentiate into memory cells. Lastly, we let the rates of $CD8^+$ T cell activation, activated cell proliferation, and activated cell death, depend on a saturation function of the viral load, V

$$F(V) = \frac{V}{l + V'} \tag{3}$$

where the parameter l determines the amount of antigen needed to generate half-maximal stimulation. Hence, a low value of l would lead to earlier antigen stimulation. This function is thus a way to define a pseudo-delay in the $CD8^+$ response due to antigen availability, and replaces the explicit delay, τ, in the activation of the effector cells in the model given by equation (2). We note however, that we no longer have a true delay, since $CD8^+$ T-cells start expanding from time zero, albeit at a slower rate early on. The function $F(V)$ takes values between 0 and 1, corresponding to proliferation of activated cells when $F(V) \approx 1$, and death by apoptosis of activated cells when $F(V) \approx 0$. A similar approach for modeling antigen-specific $CD8^+$ T cells responses was proposed by De Boer *et al.* (Boer et al., 2001) for acute lymphocytic choriomeningitis virus (LCMV) infection in mice. Incorporating these dynamics of $CD8^+$ T cell response into (2) the following system of differential equations results

$$\begin{aligned}
\frac{dT}{dt} &= r(T + I_1)(1 - \frac{T + I_1 + I_2}{T_{max}}) - kVT + \rho_1 I_1,\\
\frac{dI_1}{dt} &= kVT - (\rho_1 + z)I_1 - \mu I_1 E + \rho_2 I_2,\\
\frac{dI_2}{dt} &= rI_2(1 - \frac{T + I_1 + I_2}{T_{max}}) + zI_1 - \rho_2 I_2 - \mu I_2 E,\\
\frac{dV}{dt} &= p_1 I_1 + p_2 I_2 - cV,\\
\frac{dE}{dt} &= s_N - \omega NF(V) - d_N N,\\
\frac{dE}{dt} &= (\omega N + r_E E)F(V) - (1 - F(V))d_E E.
\end{aligned} \tag{4}$$

We used literature values for the parameters that describe the naive precursor population (Table 1). Fitting the viral load of patient 2, we found that l was approximately 4000 copies ml^{-1}. We then fixed $l = 4000$ for all patients and estimated the remaining parameters by fitting the model to the data (Figure 8). On average, it took about 29 days for V to reach 4000 copies ml^{-1}, slightly longer than the average for the delay found above ($\tau = 23$ days). Choosing different values for l between 10^3 and 10^4 did not lead to a noticeable improvement in the fits. On the basis of the Akaike information criterion (AIC), we note there is a loss in the quality of the viral DNA fits between this model and the model given by equation (2) for all patients except patients 3 and 6 (compare the last columns of Tables 2 and 3(d)). In addition, for several of the patients, this model predicts a viral rebound, not seen in the data. Moreover, the CD8$^+$ T cell concentration increases before any changes in ALT and stays elevated for a long time, since near maximal activation of effector cells occurs for viral loads well below the peak. Thus, the empirical agreement between the ALT profile and the activated effector cell population, E, is not as good in this model, as in the original model given by equation (2). However, since ALT is not fitted, we can not assess the statistical significance of this poorer agreement. Lastly, if we consider the death rate of effector cells E to be independent of the saturation function $F(V)$, *i.e.* replace $(1 - F(V))d_E E$ with $d_E E$, we cannot reproduce the dynamics of effector cell expansion hinted at by the ALT data (not shown).

4.5 Liver regeneration

The model given by equation (2) predicts the infection of most liver cells, many of which are killed by effector cells. As a result, using model (2) with the default value for the hepatocyte proliferation rate, $r = 0.01$ day^{-1} (Table 1) we obtain up to 99% hepatocyte loss at the peak of the infection. This is unrealistic and would lead to the death of the patient. To compensate for the hepatocyte death, we let the proliferation rate of both uninfected and infected cells be higher, choosing r up to 5 day^{-1}. This leads to the generation of a large number of new target cells that revive the infection (Figure 9), and consequently to a poor fit due to the resurgence in the viral load. When $r = 0.01$ day^{-1}, as in uninfected individuals, the rebound of the virus is controlled due to lack of target cells. Thus, it seems that low values of r are needed for the model given equation (2) to fit the data. To test this we allowed r to be a free parameter and refit the data. We obtained even lower values of r than the one used in our baseline analysis, with a minimum of $r = 5\times10^{-6}$ day^{-1} in patient 4.

5 Discussion

We developed mathematical models of HBV viral dynamics that account for important biological features: cytolytic and non-cytolytic immune responses, hepatocyte proliferation and the role of different families of infected cells. We used these models and the data from seven acutely infected patients to test several infection related hypothesis.

In previous models, the effects of HBV specific $CD8^+$ T-cells were incorporated indirectly, either as a higher constant death rate of infected hepatocytes (Tsiang et al., 1999;Lewin et al., 2001), or as a function that depends on the ALT concentration levels (Murray et al., 2005;Colombatto et al., 2006). In this study we designed a model incorporating both cytolytic and non-cytolytic immune responses. The model, as well as the ALT data, suggest that non-cytopathic mechanisms have an effect early in infection when the effector cell population is small and its effect is limited. However, as formulated here, the non-cytolytic response, which leads to the cure of infected cells, is unable to mediate viral clearance. Thus the cell-mediated cytolytic immune response is critical for driving the viral levels down post the peak in viral levels. That this effect is seen mainly post viral peak may be due to the need for high viral levels to stimulate the cell-mediated response or due to delays in mounting a cell-mediated response (Davenport et al., 2004). In the present work, a delayed expansion of cytolytic effector cells seems to be crucial, since when we replace it by a model where activation and expansion is dependent on antigen levels, we generally obtain worse fits to the data. If responses decline with antigen levels, then virus can expand when $CD8^+$ T cells are low and reestablish infection. In any event, the late cytolytic response is critical. Indeed, if we suppress the cytolytic immune response by setting the cytolytic killing rate $\mu = 0$, the viral load in model (2) stabilizes at a high steady state level and viral clearance does not occur (Figure 10), in disagreement with the data. This is the case, because in this model the non-cytolytic immune response continuously generates new susceptible cells, maintaining the source of new infected cells and virus. Indeed, the impact of regeneration of uninfected cells is an important issue in trying to understand clearance of acute infections.

In model (2) the peak of effector cells occurs very close to the observed peak in ALT and the effector cell dynamics follow the ALT data very closely. This result suggests that hepatocyte killing may be proportional to the ALT level as assumed in some other models (Murray et al., 2005;Colombatto et al., 2006). Further, because the ALT data was not used in our data fitting procedure, this agreement between ALT and the effector cell dynamics suggests that the model is accurately capturing the dynamics of infected cell death.

Biological studies have suggested that both cytolytic and non-cytolytic immune responses may be $CD8^+$ T cell mediated (Thimme et al., 2003). In our models the effector cell population is small when the viral load starts decreasing (Figure 3) and its effect is not felt until later when further population expansion has occurred. Therefore, any putative non-cytolytic effect of these specific effector cells is mostly negligible in our model. It may be that models that include cytokine secretion by the effector cells can exhibit a more important role for them when the $CD8^+$ population size is small. Further work is needed to elucidate this (Ciupe et al., 2007).

Our model predicts that at the peak of infection up to 99% of hepatocytes are infected (Figure 4). The viral production rate is higher in the cells infected with multiple copies of cccDNA, which dominate the pool of infected cells at the peak of infection. There was no statistically significant improvement in the model due to the presence of the second family of infected cells when fitting the model to the experimental data. However, biologically there is clearly heterogeneity in cccDNA copy number (Tuttleman et al., 1986;Wieland et al., 2004;Zhang et al., 2003).

Our models suggest that the cccDNA accumulation in infected hepatocytes may be induced by multiple infections of the same hepatocyte rather than or in addition to continued cccDNA synthesis within an infected cell. Both scenarios for cccDNA accumulation are compatible with the available HBV DNA kinetic data. Direct measurements of cccDNA levels per cell or other experiments in which superinfection is blocked are needed to further clarify the mechanisms of cccDNA accumulation.

Another point that needs clarification is the role of replication of infected hepatocytes in maintaining liver size. Previous models have ignored the kinetics of liver regeneration (Nowak et al., 1996;Tsiang et al., 1999;Lewin et al., 2001) or have assumed instantaneous replacement of killed hepatocytes by requiring the total number of hepatocytes to be constant (Murray et al., 2005;Colombatto et al., 2006). Our model accounts for the finite rate of proliferation of both uninfected and infected cells. However, in the model given by equation (2) up to 99% of hepatocytes were killed at the peak of infection. This loss is not realistic and suggests that other processes, not included in the model are significant. An increase in the proliferation rate of hepatocytes leads to viral rebound due to generation of new target cells. Future studies are needed to explain liver integrity while controlling the viral rebound. A possibility is that not all hepatocytes are susceptible to infection. If only a small fraction of cells were infectable (say 10%) then their loss would not have fatal consequences. Our models do not allow us to differentiate this possibility from the case where all hepatocytes are available for infection. However, HBV infection in animal models, such as the chimpanzee and woodchuck, suggest that essentially all hepatocytes stain positive for viral antigens at the peak of infection (Guidotti et al., 1999;Summers et al., 2003). Thus, there is no apparent bar to viral entry and viral protein production. Two other scenarios that we are exploring through modeling are the role of neutralizing antibodies in preventing the late spread of infection when target cells regenerate (ms. in preparation), and the possibility that cells once cured of infection are refractory to reinfection for some period of time (Ciupe et al., 2007).

Initial models of HBV infection were built upon earlier HIV models. However, HBV and HIV infections are quite different. HBV infection is spontaneously cleared in a majority of infected individuals, whereas HIV is not. Why some individuals clear HBV and others do not remains unclear. Here we have presented models of HBV infection that involve many features not present in HIV models, such as the consideration of non-cytolytic immune responses and the proliferation of infected cells. Modeling HBV infection provides new challenges, but as we have attempted to show here modeling can help reveal some of the underlying biological principles involved in determining whether a viral infection is cleared or becomes chronic.

Acknowledgements

Portions of this work were done under the auspices of the US Department of Energy under contract DE-AC52-06NA25396. We also acknowledge support from NIH grants RR06555 and RR18754-02 (COBRE program from NCRR), and grant RGP0010/2004 from the Human Frontiers Science Program. The research of P.W.N. and S.C. was supported in part by a Career Award at the Scientific Interface from the Burroughs Wellcome Fund. We are also very grateful to an anonymous referee, whose comments substantially improved this manuscript.

References

Ahmed R, Gray D. Immunologycal memory and protective immunity: understanding their relation. Science 1996;272:54–60. [PubMed: 8600537]

Asano M, Ahmed R. CD8 T cell memory in B cell-deficient mice. J Exp Med 1996;183:2165–2174. [PubMed: 8642326]

Banks HT, Fitzpatrick BG. Statistical methods for model comparison in parameter estimation problems for distributed systems. J Math Biol 1990;28:501–527.

Boer RD, Oprea M, Antia R, Murali-Krishna K, Ahmed R, Perelson A. Recruitment times, proliferation, and apoptosis rates during the CD8+ T-cell response to lymphocytic choriomeningitis virus. J Virol 2001;75:10663–10669. [PubMed: 11602708]

Butz E, Bevan MJ. Massive expansion of antigen-specific CD8+ T cells during an acute virus infection. Immunity 1998;8:167–175. [PubMed: 9491998]

Chisari F, Ferrari C. Hepatitis B virus immunopathogenesis. Annu Rev Immunol 1995;13:29–60. [PubMed: 7612225]

Ciupe SM, Ribeiro RM, Nelson PW, Dusheiko G, Perelson AS. The role of cells refractory to productive infection in acute hepatitis b viral dynamics. Proc Natl Acad Sci USA. 2007To appear

Ciupe S, de Bivort B, Bortz D, Nelson P. Estimates of kinetic parameters from HIV patient data during primary infection through the eyes of three different models. Math Biosci 2006;200:1–27. [PubMed: 16469337]

Colombatto P, Civitano L, Bizzarri R, Oliveri F, Choudhury S, Gieschke R, Bonino F, Brunetto MR. A multiphase model of the dynamics of HBV infection in HBeAg-negative patients during pegylated interferon-α2a, lamivudine and combination therapy. Antiviral Therapy 2006;11:197–212. [PubMed: 16640101]

Davenport M, Ribeiro R, Perelson A. Kinetics of virus-specific $CD8^+$ T cells and the control of human immunodeficiency virus infection. J Virol 2004;78:10096–10103. [PubMed: 15331742]

Flynn K, Belz G, Altman J, Ahmed R, Woodland D, Doherty P. Virus-specific $CD8^+$ T cells in primary and secondary influenza pneumonia. Immunity 1998;8:683–691. [PubMed: 9655482]

Gilles Feutren BL, Bach JF. Immune lysis of hepatocytes in culture: Accurate detection by aspartate aminotransferase release measurement. J Immunol Meth 1984;75:85–94.

Guidotti L, Chisari F. Immunobiology and pathogenesis of viral hepatitis. Annu Rev Pathol Dis 2006;1:23–61.

Guidotti L, Rochford R, Chung J, Shapiro M, Purcell R, Chisari F. Viral clearance without destruction of infected cells during acute HBV infection. Science 1999;284:825–829. [PubMed: 10221919]

Lau G, Tsiang M, Hou J, Yuen S, Carman W, Zhang L, Gibbs C, Lam S. Combination therapy with lamivudine and famciclovir for chronic hepatitis B infected Chinese patients: a viral dynamics study. Hepatology 2000;32:394–399. [PubMed: 10915748]

Lau L, Jamieson BD, Somasundaram T, Ahmed R. Cytotoxic T-cell memory without antigen. Nature 1994;369:648–652. [PubMed: 7516038]

Lewin S, Ribeiro R, Walters T, Lau G, Bowden S, Locarnini S, Perelson A. Analysis of hepatitis B viral load decline under potent therapy:complex decay profiles observed. Hepatology 2001;34:1012–1020. [PubMed: 11679973]

Murray JM, Wieland S, Purcell R, Chisari F. Dynamics of hepatitis B virus clearance in chimpanzees. Proc Natl Acad Sci USA 2005;102:17780–17785. [PubMed: 16306261]

Nelson PW, Murray JD, Perelson AS. A model of HIV-1 pathogenesis that includes an intracellular delay. Math Biosci 2000;163:201–215. [PubMed: 10701304]

Nowak M, Bonhoeffer S, Hill A, Boehme R, Thomas H, McDade H. Viral dynamics in hepatitis B infection. Proc Natl Acad Sci USA 1996;93:4398–4402. [PubMed: 8633078]

Ogg G, McMichael A. HLA-peptide tetrametic complex. Curr Opin Immunol Today 1998;10:393–396.

Payne R, Nowak M, Blumberg B. A cellular model to explain the pathogenesis of infection by the hepatitis B virus. Math Biosci 1994a;123:25–58. [PubMed: 7949745]

Payne R, Nowak M, Blumberg B. A cellular model to explain the pathogenesis of infection by the hepatitis B virus. Math Biosci 1994b;123:25–58. [PubMed: 7949745]

Perelson AS, Herrmann E, Micol F, Zeuzem S. New kinetic models for the hepatitis c virus. Hepatology 2005;42:749–754. [PubMed: 16175615]

Perelson A, Neumann A, Markowitz M, Leonard J, Ho D. HIV-1 dynamics in vivo: Virion clearance rate, infected cell life-span, and viral generation time. Science 1996;271:1582–86. [PubMed: 8599114]

Perelson A, Ribeiro R. Hepatitis B virus kinetics and mathematical modeling. Sem Liv Dis 2004;24:11–15.

Perelson A. Modelling viral and immune system dynamics. Nature Rev Immunol 2002;2:28–36. [PubMed: 11905835]

Phillips A. Reduction of HIV concentration during acute infection: independence from a specific immune response. Science 1996;271:497–499. [PubMed: 8560262]

Ribeiro R, Lo A, Perelson A. Dynamics of hepatitis B virus infection. Microbes and Infection 2002;4:829–835. [PubMed: 12270730]

Sherlock, S.; Dooley, J. Diseases of the Liver and Biliary System. 11th. Blackwell Science; Oxford: 2002.

Stafford M, Corey L, Cap Y, Daar E, Ho D, Perelson A. Modeling plasma virus concentration during primary HIV infection. J Theoret Biol 2000;203:285–301. [PubMed: 10716909]

Summers J, Jilbert AR, Yang W, Aldrich CE, Saputelli J, Litwin S, Toll E, Mason WS. Hepatocyte turnover during resolution of a transient hepadnaviral infection. Proc Natl Acad Sci USA 2003;100:11652–11659. [PubMed: 14500915]

Thimme R, Bukh J, Spangenberg HC, Wieland S, Pemberton J, Steiger C, Govindarajan S, Purcell R, Chisari FV. Viral and immunological determinants of hepatitis C virus clearance, persistence, and disease. Proc Natl Acad Sci USA 2002;99:15661–15668. [PubMed: 12441397]

Thimme R, Wieland S, Steiger C, Ghrayeb J, Reimann K, Purcell R, Chisari F. CD8+ T cell mediate viral clearance and disease pathogenesis during acute hepatitis B virus infection. J Virol 2003;77:68–76. [PubMed: 12477811]

Tsiang M, Rooney J, Toole J, Gibbs C. Biphasic clearance kinetics of hepatitis B virus from patients during adefovir dipivoxil therapy. Hepatology 1999;29:1863–1869. [PubMed: 10347131]

Tuttleman J, Pourcel C, Summers J. Formation of the pool of covalently closed circular viral DNA in hepadnavirus-infected cells. Cell 1986;47:451–460. [PubMed: 3768961]

Webster G, Hallett R, Whalley S, Meltzer M, Balogun K, Brown D, Farrington C. Molecular epidemiology of a large outbreak of hepatitis B linked to autohaemotherapy. Lancet 2000a;356:379–384. [PubMed: 10972370]

Webster G, Reignat S, Maini M, Whalley S, Ogg G, King A, Brown D. Incubation phase of acute hepatitis B in man: dynamic of cellular immune mechanism. Hepatology 2000b;32:1117–1124. [PubMed: 11050064]

Whalley S, Murray J, Brown D, Webster G, Emery V, Dusheiko G, Perelson A. Kinetics of acute hepatitis B virus infection in humans. J Exp Med 2001;193:847–853. [PubMed: 11283157]

Wieland S, Spangenberg H, Thimme R, Purcell R, Chisari F. Expansion and contraction of the hepatitis B virus transcriptional template in infected chimpanzees. Proc Natl Acad Sci USA 2004;101:2129–2134. [PubMed: 14764900]

Zhang YY, Zhang BH, Theele D, Litwin S, Toll E, Summers J. Single-cell analysis of covalently closed circular DNA copy numbers in a hepadnavirus-infected liver. Proc Natl Acad Sci USA 2003;100:12372–12377. [PubMed: 14528003]

Zimmerman C, Brduscha-Riem K, Blaser C, Zinkernagel RM, Pircher H. Visualization, characterization, and turnover of CD8+ memory T cells in virus-infected hosts. J Exp Med 1996;183:1367–1375. [PubMed: 8666895]

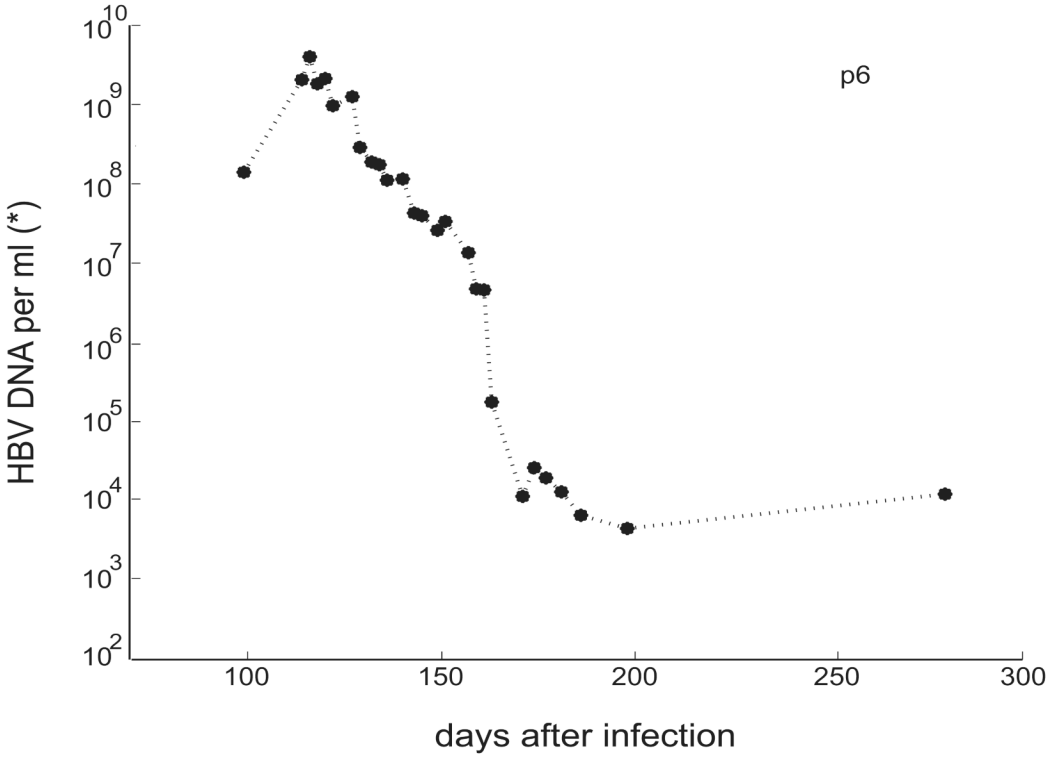

Figure 1.
The decay of HBV-DNA virus titer during acute infection of one patient.

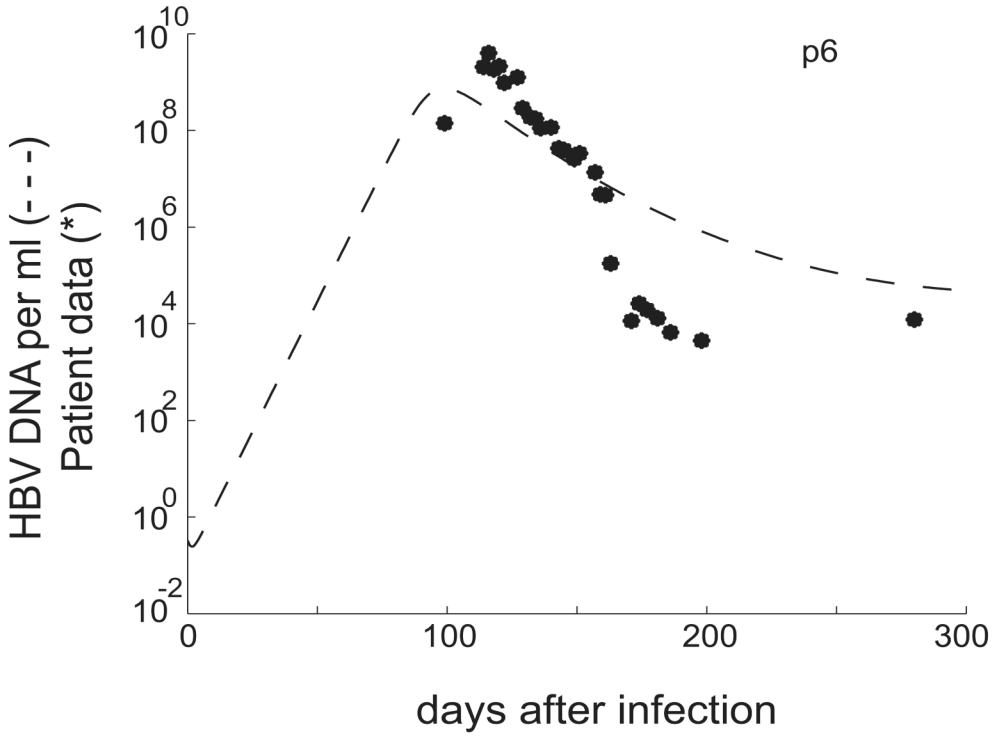

Figure 2.
Results of fitting the model given by equation (1) to the data for patient 6. We use the initial conditions given in Table 1 and fit all the parameters, except $\lambda = dT_0$. The results predict viral steady state levels higher than observed and a poor fit to the data at the peak. The results are characteristic of all patients.

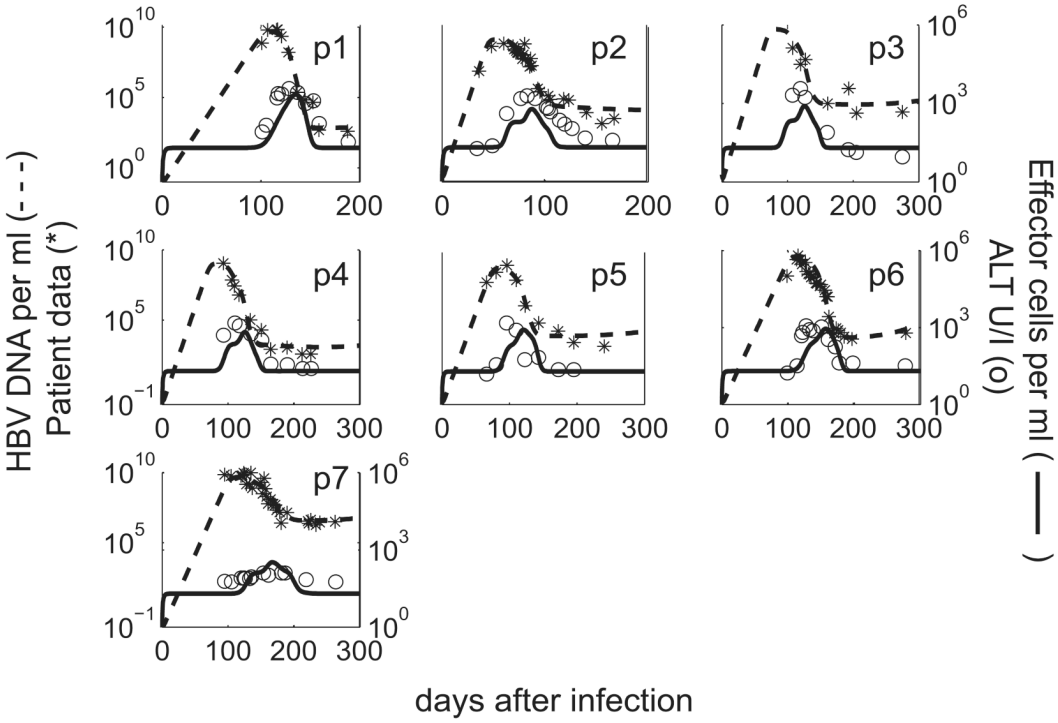

Figure 3.

Results of fitting the model to each patient's HBV DNA data and the relationship between effector cells and serum ALT during the acute phase of the infection. The best fit of the model (dashed line) to HBV DNA patient data (*). The measured serum ALT (o), which was not used in data fitting, compares well with the predicted dynamics of the HBV-specific $CD8^+$ T-cell response (solid line). Note that the peak of the effector cell response occurs after 90% viral load reduction.

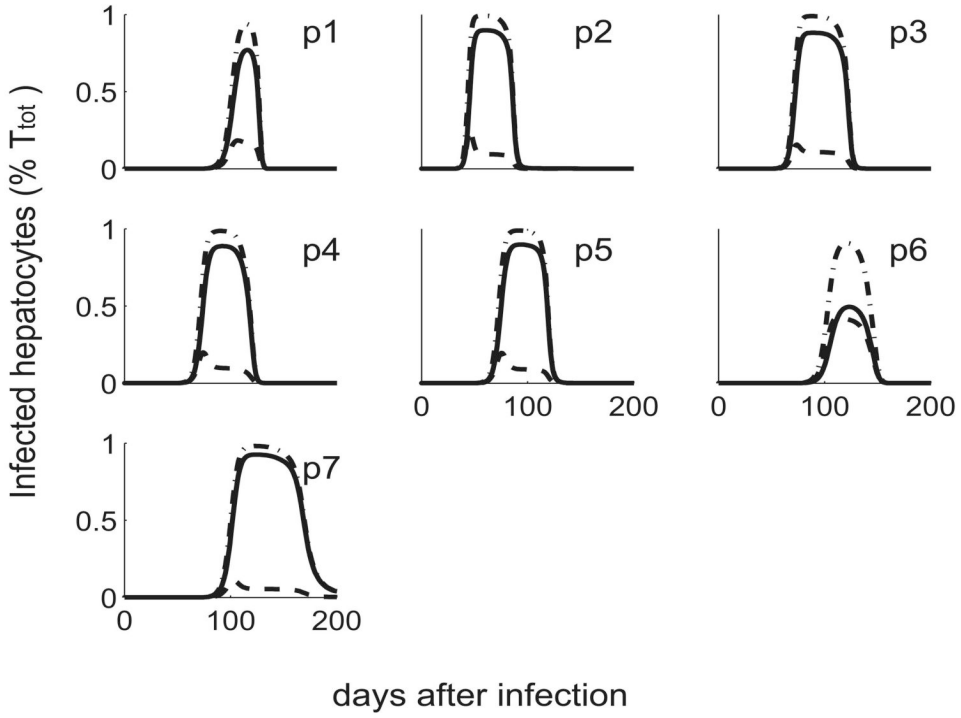

Figure 4.
Infected hepatocyte levels (fraction of T_{total}). The number of cells with one cccDNA, I_1, (dashed lines) is smaller than the number of cells with multiple, I_2, cccDNA (solid lines). The dash-dotted line represents the total number, $I_1 + I_2$, of infected cells as a fraction of the total number of hepatocytes.

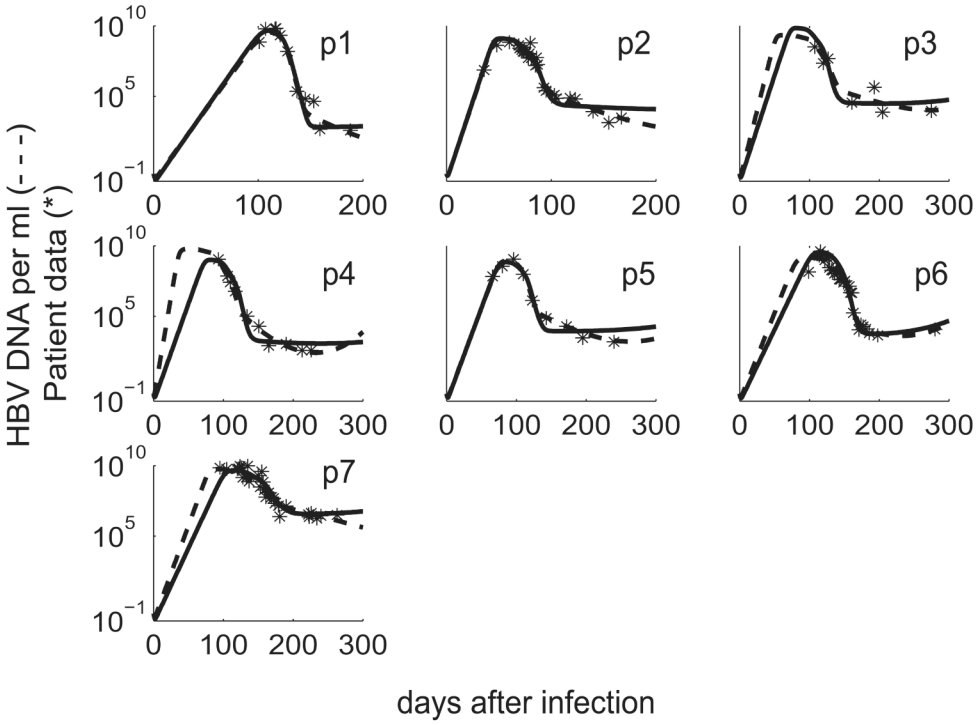

Figure 5.
Best fit of the model given by equation (2) (solid line) and the model with multiple infectious events (dashed line) to the data (*).

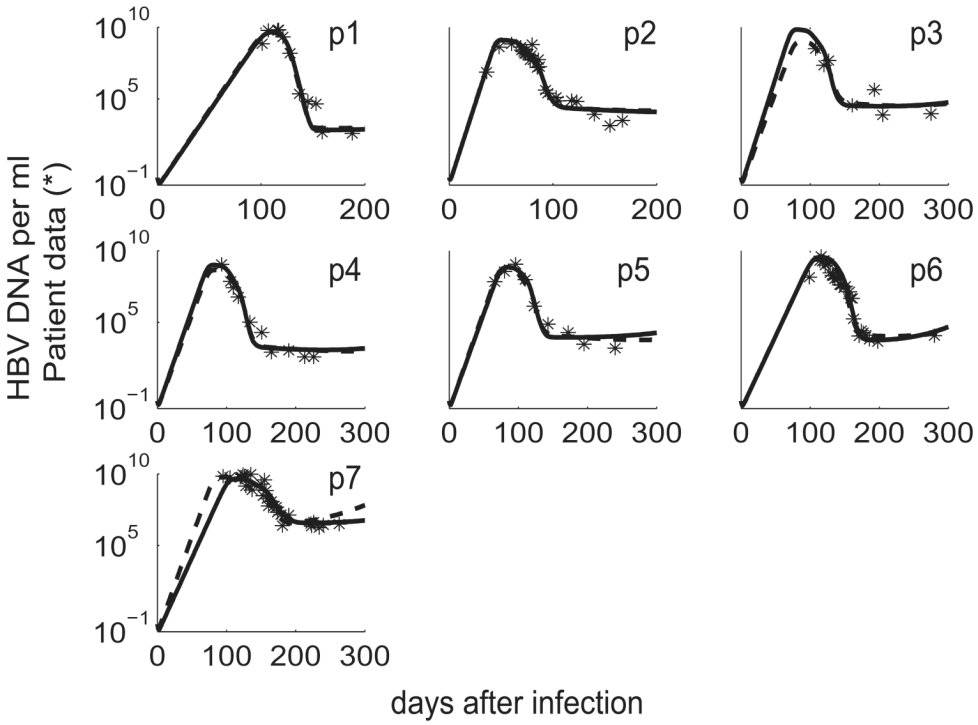

Figure 6.
Best fit of the model given by equation (2) (solid line) and the model with recovery rates dependent on effector cells (dashed line) to the data (*).

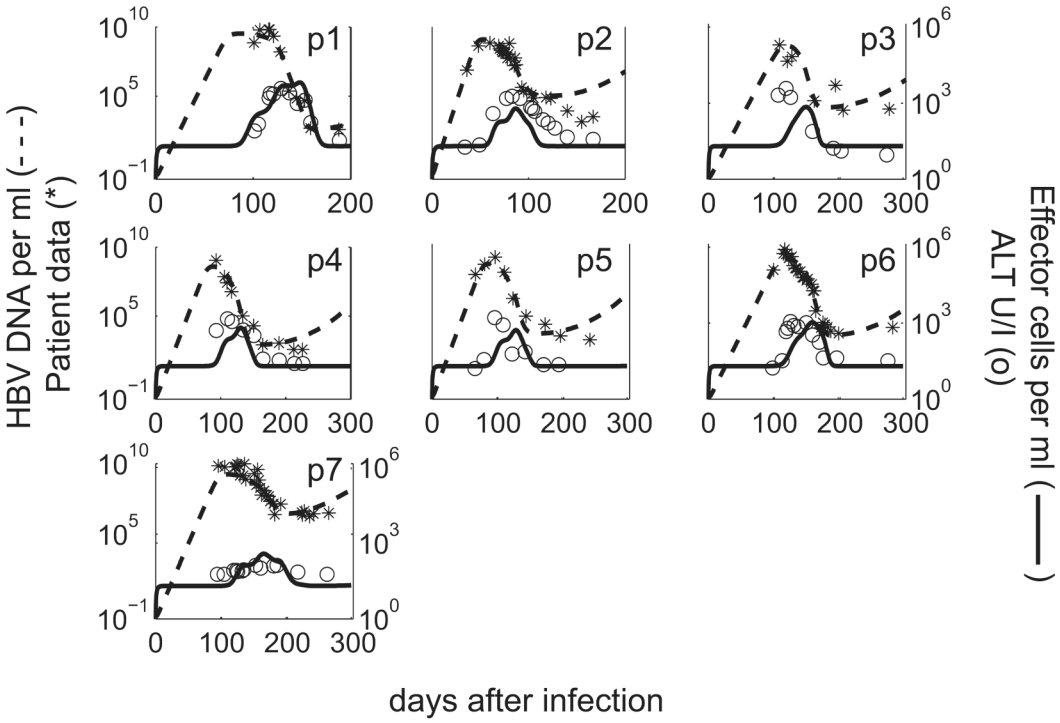

Figure 7.
Results of fitting the model with one class of infected cells to the data. The best fit of the model (dashed line) to HBV DNA patient data (*). The measured serum ALT (o), which was not used in data fitting, compares well with the predicted dynamics of the HBV-specific $CD8^+$ T-cell response (solid line).

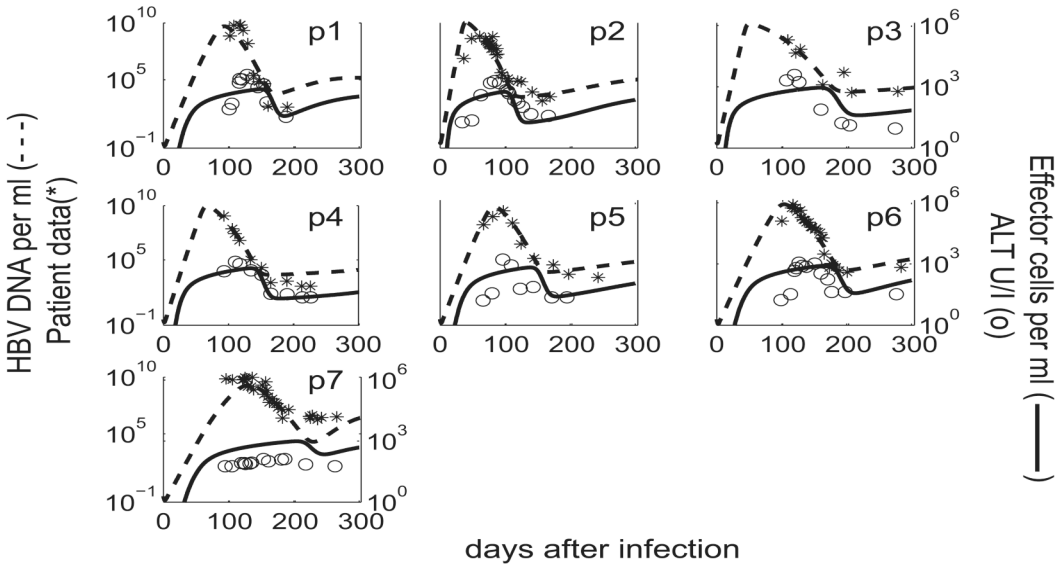

Figure 8.
Results from fitting the model given by equation (4) (dashed lines) to the data (*). We note a worse match of the measured serum ALT (o), which was not used in data fitting and the predicted HBV-specific $CD8^+$ T-cells (solid line).

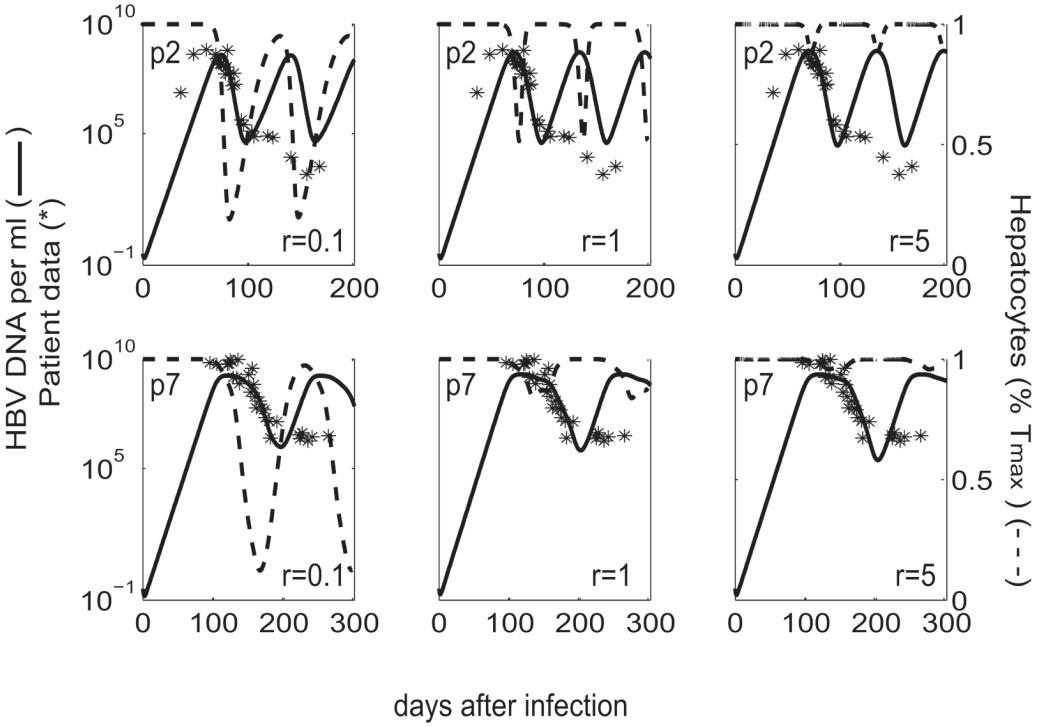

Figure 9.
Results of fitting model given by equation (2) (solid line) to the data (*) and the total hepatocytes as percent of T_{max} (dashed line) for $r = 0.1$ day^{-1}, $r = 1$ day^{-1}, and $r = 0\ 5$ day^{-1}. Hepatocyte destruction is reduced when we allow for higher proliferation rates. Results are presented for patients 2 and 7.

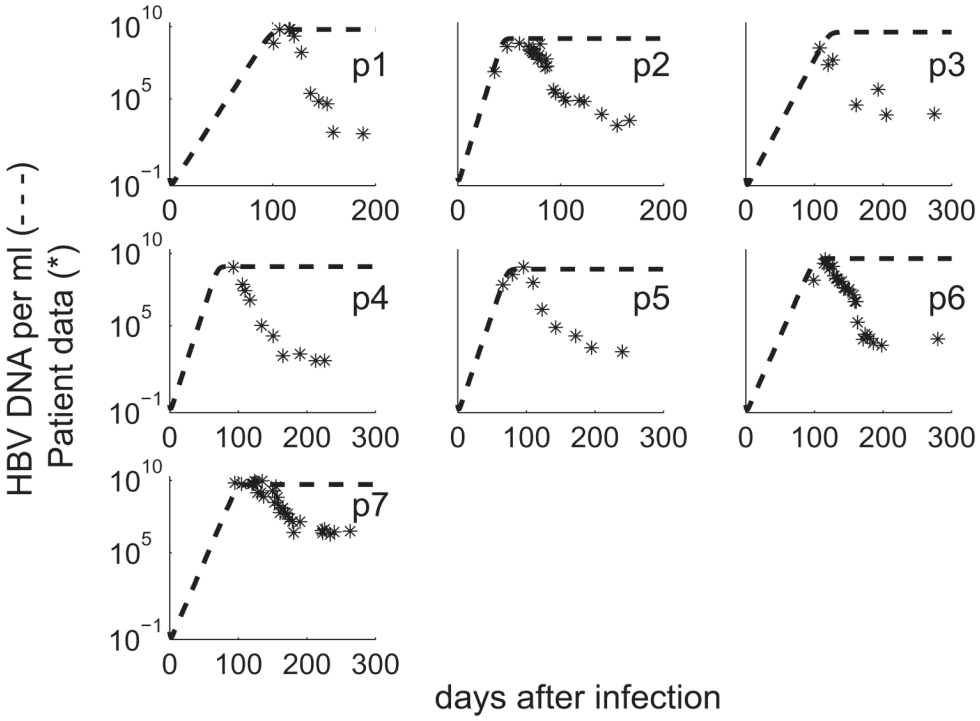

Figure 10.
Results of fitting model given by equation (2) with $\mu = 0$ (dashed line) to the data (*).

Table 1

Parameter values used in the HBV-DNA kinetic model. We normalize the liver cell population of 2×10^{11} so that we consider the cells responsible for producing virus in one ml. For that we assume HBV DNA can distribute throughout the 15 liters of extracellular fluid, in an average 70 kg person. We also consider the amount of HBV contaminated blood that initiated infection of 10^3 HBV DNA to be diluted in 3 liters of serum, rather than the 15 liters of extracellular fluid (since this inoculum was injected directly into the blood circulation).

Parameter	Description	Value	Reference
r	uninfected cells proliferation rate	0.01 day^{-1}	
T_{max}	max hepatocyte density	13.6×10^6 cells/ml	Sherlock and Dooley, 2002
c	clearance rate	0.67 $days^{-1}$	Nowak et al., 1996;Tsiang et al., 1999
s	source term, lymphocytes	10 cells/ml/day	Webster et al., 2000b
d_E	death rate, lymphocytes	0.5 day^{-1}	Ahmed and Gray, 1996
T_0	initial, uninfected hepatocyte	13.6×10^6 cells/ml	
I_{10}, I_{20}	initial, infected hepatocyte	0 cells/ml	
V_0	initial, virus	0.33 particles/ml	Whalley et al., 2001
E_0[2]	initial, lymphocytes	20 cells/ml	Webster et al., 2000b
s_N	source term, naive lymphocytes	10 cells/ml/day	Webster et al., 2000b
ω	activation rate, lymphocytes	1 day^{-1}	Boer et al., 2001
l	antigenic stimulation, lymphocytes	4000 particles/ml	
d_N	death rate, naive lymphocytes	0.5 day^{-1}	Ahmed and Gray, 1996
N_0	initial, naive lymphocytes	20 cells/ml	

[1] For model (4) $E_0 = 0$

Table 2

Estimates for the parameters in the model given by equation 2. Parameters are described in section 2 of the text. J represents the square root of the sum of squared residuals, and AIC is the Akaike information criterion.

Patient	μ ml/cell $d^{-1}\times10^{-4}$	α ml/cell $d^{-1}\times10^{-7}$	z d^{-1}	τ d	ρ_1 d^{-1}	ρ_2 d^{-1}	p_1 vir/cell d^{-1}	p_2 vir/cell d^{-1}	k ml/vir $d^{-1}\times10^{-10}$	J	AIC
1	5.8	7.3	0.81	15.1	0.071	0.18	34	376	0.7	2.57	12.3
2	9.9	3.6	0.59	19.6	0.064	0.06	**75**	73	6.7	2.33	−15.2
3	6.9	4.1	0.98	24.9	0.05	0.11	201	428	0.8	2.15	15.1
4	8.9	4.5	0.52	24.9	0.05	0.057	62	62	4.2	2.05	9
5	5.4	3.9	0.51	20.7	0.05	0.051	29	42	6.7	1.76	8.4
6	6.4	5.2	0.22	24.9	0.05	0.18	232	232	0.8	3.28	−6.8
7	5.9	2.3	0.84	29.9	0.11	0.05	83	275	0.9	2.89	−18.1
median	6.4	4.2	0.59	24.9	0.05	0.06	75	232	0.9		
mean	7.0	4.4	0.64	22.9	0.06	0.1	102	213	3.0		
stdev	1.7	1.5	0.25	4.8	0.02	0.05	81	157	2.8		

Table 3

Parameter estimates in the alternative models: (a) multiple infection induced by superinfection; (b) cure of infected cells depends on cytokine production by HBV-specific $CD8^+$ T-cells; (c) only one class of infected cells; (d) we incorporate the activation of HBV-specific lymphocytes. Parameters are described in sections 2 and 4.1-4.5. P-values are for comparison of the model in Table 2 with its sub-models here (Banks and Fitzpatrick, 1990). AIC are for comparison with model in Table 2, when the models are not nested. Lower AIC indicates better fit to the data.

(a)	*Pat*	μ ml/cell $d^{-1}\times10^{-4}$	α ml/cell $d^{-1}\times10^{-7}$	r_E d^{-1}	z d^{-1}	τ d	ρ_1 d^{-1}	ρ_2 d^{-1}	ρ'_1 ml/cell $d^{-1}\times10^{-6}$	ρ'_2 ml/cell $d^{-1}\times10^{-6}$	p_1 vir/cell d^{-1}	p_2 vir/cell d^{-1}	k ml/vir $d^{-1}\times10^{-10}$	AIC
	1	5.5	6.6	-	0.7×10^{-10}	12.1	0.12	0.11	-	-	211	287	1.1	9.7
	2	9.9	3.0	-	4.0×10^{-10}	17.8	0.08	0.07	-	-	69	70	7.7	−30.6
	3	1.8	3.1	-	4.4×10^{-10}	24.9	0.06	0.07	-	-	109	112	3.9	11.5
	4	1.6	3.3	-	1.1×10^{-10}	24.9	0.19	0.14	-	-	151	339	5.6	−0.41
	5	2.7	3.0	-	3.9×10^{-10}	13.9	0.09	0.10	-	-	41	52	7.0	0.26
	6	1.0	4.5	-	1.3×10^{-10}	24.9	0.12	0.10	-	-	81	81	3.6	−21.7
	7	1.9	2.1	-	8.4×10^{-10}	24.9	0.06	0.05	-	-	278	288	1.0	−19.1
														P-val
(b)	1	8.0	7.6	-	0.36	16.2	0.10	0.12	5.4	16	126	410	0.7	0.91
	2	9.9	3.6	-	0.67	19.3	0.05	0.11	5.3	0.6	74	75	6.5	1.0
	3	9.9	3.2	-	0.38	24.9	0.06	0.05	1.2	0.5	34	68	4.7	0.26
	4	9.9	4.1	-	0.91	24.9	0.06	0.05	1.6	3.2	27	28	8.5	0.3
	5	9.9	3.5	-	0.87	24.5	0.05	0.05	1.9	1.4	21	33	8.5	0.36
	6	9.8	4.3	-	0.95	24.9	0.15	0.09	5.2	4.0	158	211	0.9	0.02
	7	1.0	2.8	-	0.48	25.1	0.14	0.10	1.4	0.4	185	327	1.0	1.0
														P-val
(c)	1	1.2	8.6	-	-	24.9	0.10	-	-	-	202	-	1.6	1
	2	9.8	4.2	-	-	18.2	0.17	-	-	-	83	-	7.1	1
	3	6.9	4.5	-	-	18.8	0.05	-	-	-	22	-	7.6	0.29
	4	10	5.4	-	-	24.9	0.05	-	-	-	27	-	9.1	0.58
	5	9.9	4.5	-	-	24.9	0.05	-	-	-	26	-	9.8	0.12
	6	5.1	5.6	-	-	24.9	0.05	-	-	-	56	-	3.2	1
	7	5.0	2.7	-	-	31.8	0.06	-	-	-	114	-	1.9	0.1
				$\times10^{-4}$										AIC
(d)	1	4.3	-	9.1	0.81	-	0.05	0.05	-	-	181	999	0.3	18.9
	2	5.7	-	9.8	0.54	-	0.13	0.12	-	-	797	864	1.0	−7.8
	3	1.9	-	0.7	0.99	-	0.05	0.05	-	-	503	505	1.0	12.5
	4	3.6	-	8.2	0.86	-	0.05	0.05	-	-	52	999	0.6	9
	5	4.0	-	1.7	0.89	-	0.05	0.05	-	-	20	377	1.0	8.5
	6	2.9	-	6.2	0.40	-	0.05	0.05	-	-	22	764	0.5	−14.7
	7	4.0	-	0.04	0.91	-	0.11	0.09	-	-	722	995	0.2	19.1